Journal of the Brazilian Society of Mechanical Sciences and Engineering (2020) 42:356
https://doi.org/10.1007/s40430-020-02433-z

TECHNICAL PAPER

Multi-objective optimization of high-speed turning parameters for hardened AISI S7 tool steel using grey relational analysis

Akash Awale[1] · **Kedar Inamdar**[2]

Received: 4 June 2019 / Accepted: 25 May 2020 / Published online: 9 June 2020

Abstract

Nowadays, die manufacturing industries prefer eco-friendly machining, i.e., high-speed turning for hardened AISI S7 tool steel followed by the conventional grinding process. The effectiveness of this eco-friendly turning depends on selection of appropriate process parameters, which decides the surface integrity of machined components. Hence, the first objective of present research work is to optimize the turning parameters for lower cutting force, machining temperature, surface roughness and higher material removal rate simultaneously using grey relational analysis (GRA). ANOVA utilized to identify the significant effect of each turning parameter on the response variables. Secondly, the effects of turning parameters such as tool nose radius (R_n), cutting speed (V_c), feed rate (V_f) and depth of cut (d_c) on tool wear and finished surface topography were studied through scanning electron microscopy (SEM) and atomic force microscope (AFM). Optimal turning parameters for multi-performance responses were R_n: 1.2 mm, V_c: 450 m/min, V_f: 0.05 mm/rev and d_c: 0.2 mm. The confirmation test was conducted on the optimal parameter level. According to ANOVA, depth of cut was the major influencing factor on all response variables. AFM and SEM micrograph indicated that excellent surface quality with lower surface roughness (S_a: 64.21 nm and S_q: 90.34 nm) was observed at higher cutting speed. Flank and crater wear were observed in cutting tool faces owing to thermo-mechanical loading. Different wear mechanisms like abrasion, adhesion, built-up edge formation and chipping hammering were found in the alumina-mixed ceramic insert at higher cutting speed and depth of cut.

Keywords High-speed turning · AISI S7 tool steel · Surface topography · Tool wear · Atomic force microscope · Grey relational analysis

1 Introduction

AISI S7 tool steel is one of the important shock resistance material according to tool manufacturing industries. It is extensively used in riveting and blanking dies, master hob and various cutting tools because it has excellent thermo-mechanical properties like high impact and shock resistance, high hardenability and high toughness at elevated temperature [1]. Majority of the machined components in their application require heat treatment to enhance the wear resistance and handling the high temperature during its functioning. Hence, hardened AISI S7 tool steel (48–60 HRC) becomes the part of "difficult-to-cut" materials group like Inconel, titanium, stainless steel, hardened AISI 4340 steel due to high work hardening and low thermal conductivity [2]. Machining of "difficult-to-cut" material with achieving close-dimensional tolerance is big challenge for machine operator. On the other hand, huge petroleum-based cutting fluid was utilized during conventional machining of "difficult-to-cut" material to maintain the surface quality, which generates unfavorable effects on the environmental aspects and machine operator health in the form of skin cancer to worker, air and water pollution [3]. Hence, eco-friendly machining, i.e., high-speed turning has added considerable attention toward the above serious problem.

High-speed turning is recognized as the most effective manufacturing technique in terms of higher productivity with negligible manufacturing cost. The basic principle behind this process is machining of metal at higher cutting

Technical Editor: Adriano Fagali de Souza.

✉ Akash Awale
akashsa.rs.mec16@iitbhu.ac.in

[1] Department of Mechanical Engineering, Indian Institute of Technology (BHU), Varanasi 221005, India

[2] Department of Mechanical Engineering, Walchand College of Engineering, Sangli 416415, India

speed near about five to ten times more than conventional cutting speed, which induced large plasticity in the work material, resulting in enhancement in the material removal rate [4]. High-speed turning with advanced cutting tool that offers many substantial benefits as compared to conventional machining such as lower cutting force, free from cutting fluid, reduced power consumption, low residual stress, close-dimensional accuracy and excellent surface quality [5]. In this process, the machining performance and surface integrity of machined component are dependent on the process parameters, work material behaviors and tool-chip interaction. Hence, machining parameters were properly optimized for excellent machinability of hardened AISI S7 tool steel in the form of higher material removal rate with outstanding surface finish. Hence, Taguchi-based signal-to-noise (*S*/*N*) ratio and ANOVA techniques were used to find the optimal process parameters for individual response variable. When process parameters are optimized for multiple response variables of the same dataset, *S*/*N* ratio and ANOVA could not provide appropriate solution. To achieve high machinability criteria for hardened AISI S7 tool steel, a multi-objective optimization strategy such as grey relational analysis (GRA) is implemented in present research work.

Most of the research groups focus their research work on experimental investigation of the effect of high-speed turning on different engineering materials. Iuliano et al. [6] are possibly the first who attempted high-speed turning of aluminum-based metal matrix composite using diamond-coated carbide tool and found that important in tool life and reduction in built-edge formation. Kishawy and Elbestawi [7] investigated the effect of higher cutting speed on tool wear and residual stress during high-speed turning of hardened AISI D2 tool steel. The experimental results revealed a reduction in unfavorable tensile residual stresses with increase in cutting speed. Abukhshim et al. [8] studied the effect of high heat generation on the cutting tool-chip interface area while high-speed turning of AISI 4140 steel. They reported that cutting tool-chip interface area decreases with increase in cutting speed, resulting in the maximum amount of heat removed by deformed chip. Pawade et al. [9] studied the effectiveness of higher cutting speed in turning of superalloy, Inconel 718. They observed minimum surface damage and lower surface roughness at higher cutting speed. Thakur et al. [10] evaluated the machinability of Inconel 718 upon high-speed turning with tungsten carbide tool. They reported that excellent machinability of Inconel 718 under high-speed turning in terms of lower cutting force with outstanding surface quality. Zhou et al. [11] studied the effect of whisker-reinforced ceramic tool on surface integrity of age-hardened Inconel 718 under high-speed turning. They confirmed that ceramic tool have a longer tool life and produced minimum thermal damage on finished surface at higher cutting speed. Naskar and Chattopadhyay [12] studied the flank wear mechanism of Al_2O_3/TiC, TiCN/TiC and TiAlN ceramic inserts during high-speed turning of C20 and C80 steel. They reported that large flank wear of TiCN/TiC was observed during turning of C80 steel.

Recently, researchers adopted GRA technique for optimization of machining parameters for multi-objective response variables. Tzeng et al. [13] applied first time GRA to optimize the turning parameters for AISI D2 tool steel. Kacal and Yildirim [14] also utilized GRA to optimize the turning parameters for lower tool wear and better surface finish of AISI D6 tool steel. They reported that optimal turning parameters including cutting speed of 250 m/min, feed rate of 0.05 mm/rev and depth of cut of 0.2 mm for better machining performance on work material. Eskandari et al. [15] employed Taguchi-based GRA method to optimize the turning parameters for multiple response variables such as surface finish, tool life and material removal rate of iron-nickel-based superalloy, N-155. GRA technique applied in various manufacturing domain to optimization of process parameters including friction stir welding [16], electrical discharge drilling [17], flow forming process [18] and squeeze casting [19].

From the literature studies, it can confirm that huge research work has been already done on the effect of high-speed turning on different "difficult-to-cut" materials [7–10] and cutting tools [11, 12]. Still, no systematic study has been conducted on the effect of high-speed turning on surface integrity of hardened AISI S7 tool steel and tooling performance of alumina-mixed ceramic tool. Furthermore, few research groups attempted to use GRA technique to optimize the turning parameters for different response variables of "difficult-to-cut" material. The aim of present research work is experimentally investigating the effect of high cutting speed on machined surface topography and tool wear of alumina-mixed ceramic tool. Besides, *S*/*N* ratio and ANOVA method were adopted to determine the optimal process parameters like cutting speed, feed rate, depth of cut, tool nose radius to satisfy the individual response variables such as higher material removal rate (MRR) and lower cutting force (F_c), machining temperature (T_m) and surface roughness (R_a) while turning of work material. Finally, GRA technique was employed to optimize the high-speed turning parameters for multiple response characteristics of AISI S7 tool steel.

2 Experimental procedure

2.1 Work material and cutting tool

AISI S7 tool steel is considered as work material in the present work, which is widely used in manufacturing of blanking dies, forming dies and gauges owing to excellent

wear and shock resistance and high hardening capacity. The high-speed turning was carried out on 40 mm diameter with 150-mm-long round bars of work material. Samples were heat-treated at an out-door heat treatment facility (Metals Heat Treatment Pvt. Ltd., India) to achieve the desired uniform hardness of 48 ± 2 HRC. Before experimentation, 1 mm material was removed from the top surface of received work material to eliminate any surface defect due to heat treatment, which directly affects machining performance. The chemical composition of AISI S7 tool steel is summarized in Table 1. Experiment was performed on work material using MTAB MAXTURN Plus + CNC lathe. The technical details of this machine are as follows: position accuracy of 10 µm; run out of spindle is 10 µm; maximum spindle speed of 6000 rpm; power is 12 kW. Alumina-mixed ceramic insert (Series-CC650) containing 70% Al_2O_3 and 30% TiC with two distinct representative types of nose radius like 0.8 mm and 1.2 mm was utilized for turning of work material. These two ceramic inserts ISO designation are TNGA 160408T01020 650 and TNGA 160412T01020 650 (Sandvik, India). This insert was mounted on a tool holder of ISO designation of DCLNL 2525 M12 (Sandvik, India). The specification of cutting angle of tool holder is as follows: back rake angle of − 6°; side cutting edge angle of 95°; positive clearance angle of 11°; side rake angle of 6°; and inclination angle of − 6°. A new cutting edge was utilized for each experimental setting to study the effect of high-speed turning on tool wear. The experimental setup along with important characterization units is shown in Fig. 1.

2.2 Design of experiment

In the present study, experiments were conducted using Taguchi-based orthogonal array, which helps to find out

Table 1 Chemical composition of AISI S7 tool steel (wt.%)

C	Si	Mg	P	Su	Cr	Mo	V
0.550	0.630	0.430	0.013	0.006	3.230	1.400	0.280

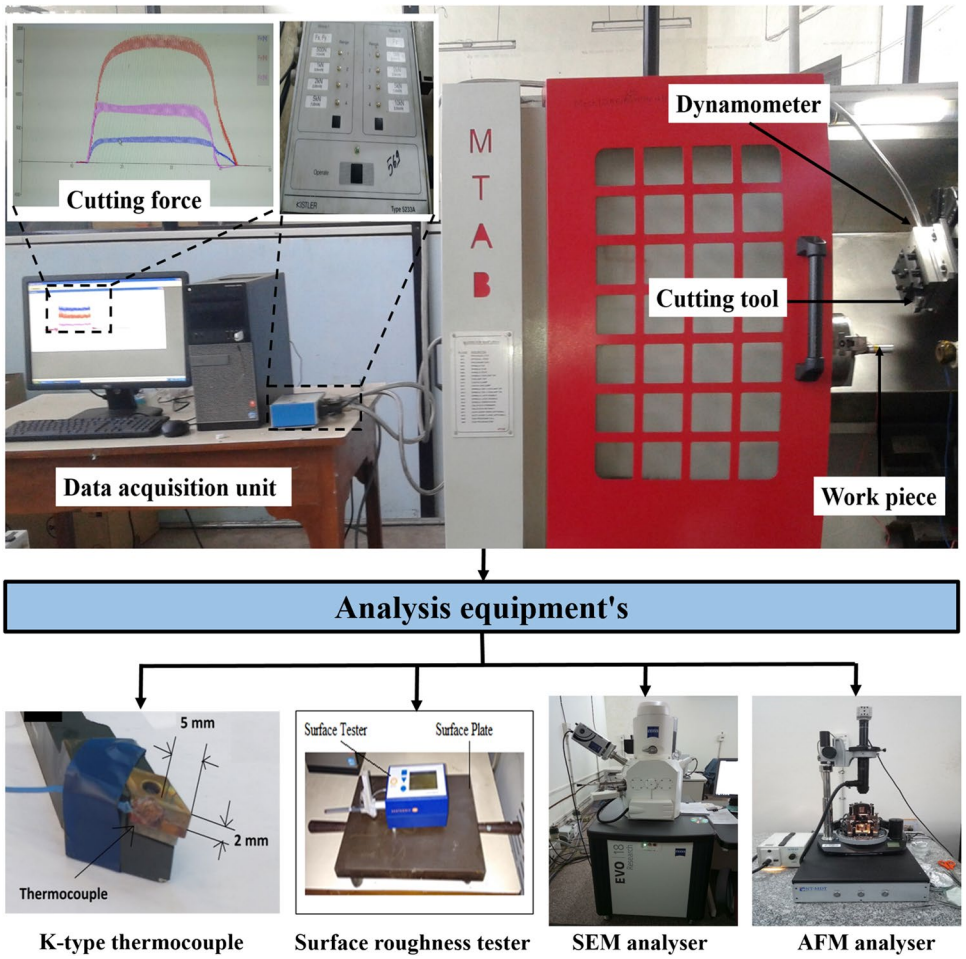

Fig. 1 Experiential setup along with important characterization units

the optimal combination of experiential sets on the basis of number of process parameters and their levels. The four turning parameters, i.e., tool nose radius, cutting speed, feed rate and depth of cut, were selected to study the machinability of AISI S7 tool steel in terms of cutting force, material removal rate, machining temperature and surface roughness under high-speed turning. Initially, a number of trial experiments were conducted on work material to decide the parameters range and their levels. The final experiment was planned according to L_{18} combined orthogonal array with two replicas. The L_{18} ($2^1 \times 3^3$) orthogonal array is selected because it has 17 degree of freedom, which is higher than 7 degree of freedom of process parameters. Besides, this array has 8 columns and 18 rows. The first column has two-level process parameters and remaining six columns have three-level process parameters, therefore two levels of tool nose radius along with three levels of rest parameters. The turning parameters and their levels are summarized in Table 2. Appearance of the finished samples with two replications is shown in Fig. 2.

2.3 Analysis equipment

Three components of cutting force were recorded and measured by using a piezo-electric Kistler dynamometer with excellent resolution of 1 mN. Cutting force signal was amplified through a charge meter (Model: 5233A). Machining temperature was measured by K-type thermocouple having a temperature range from − 100 to 1200 °C (Risepro, India). The thermocouple was mounted 5 mm away from end cutting edge and 2 mm below from face of cutting insert using brazing process. Further, samples are cleaned by ethanol. Surface roughness (R_a) was measured along to feed direction at three different locations with cutoff length of 4.8 mm and traverse length of 0.8 mm using Taylor Hobson surface roughness tester (Model: Talyrond 131). Each sample was cut near the circumference surface in the size of 10 × 10 × 5 mm by wire electrical discharge machining for studying the 2D and 3D surface topography. 2D surface micrograph and tool wear micrograph were obtained by scanning electron microscope (Zeiss EVO-18 Research). 3D surface topography with nanoscale roughness of machined sample was obtained by atomic force microscope (NT-MDTN Tegra Prima, Russia).

Table 2 Experimental parameters and their levels

Process parameters	Symbol	Level 1	Level 2	Level 3
Tool nose radius (mm)	R_n	0.8	1.2	–
Cutting speed (m/min)	V_c	400	450	500
Feed rate (mm/rev)	V_f	0.05	0.1	0.15
Depth of cut (mm)	d_c	0.2	0.4	0.6

3 Results and discussion

3.1 Taguchi-based signal-to-noise ratio

In signal-to-noise (*S*/*N*) ratio, the signal is denoted as controllable factors and noise is denoted as uncontrollable factors. *S*/*N* ratio is used to predict the performance of controllable factors with the existence of uncontrollable factors [20]. Three different types of *S*/*N* ratio function were used to select better performance characteristics like higher-to-better, nominal-to-better and lower-to-better. Generally, better machinability of AISI S7 tool steel was considered at maximum material removal rate and minimum cutting force, machining temperature and surface roughness. Hence, higher-to-better function was applied on MRR, and small-to-better function was used for cutting force, machining

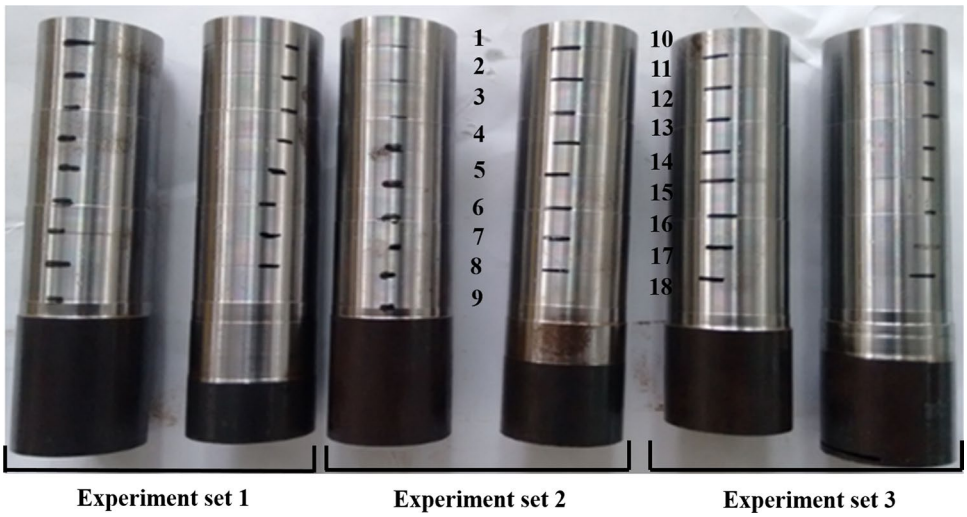

Fig. 2 Appearance of the finished samples

temperature and surface roughness. It can be calculated by Eqs. 1, 2:

$$(S/N)_{ij} = -10\log\frac{1}{n}\left(\sum_{k=1}^{n} x_{ij}^2\right) \quad (1)$$

$$(S/N)_{ij} = -10\log\frac{1}{n}\left(\sum_{k=1}^{n} \frac{1}{x_{ij}^2}\right), \quad (2)$$

whereas $(S/N)_{ij}$ is *S*/*N* ratio of *i*th response variables in the *j*th test. *n* is denoted as number of tests, and x_{ij} is denoted as predicted value of *i*th response variable in the *j*th test. The L_{18} orthogonal array of process parameters along with response variables is listed in Table 3. The highest *S*/*N* ratio represents the optimal process parameters for specific response variable with minimum error. The *S*/*N* ratio of all respective response variables is illustrated in Table 4. Further, optimal turning parameter is calculated by mean of *S*/*N* ratio and presented in Table 5. Optimal process parameters for the better cutting force and surface roughness during high-speed turning was obtained at 1.2 mm tool nose radius, 450 m/min cutting speed, 0.05 mm/rev feed rate and 0.2 mm depth of cut. Similarly, for machining temperature analysis selected best turning parameters includes 0.8 mm tool nose radius, 450 m/min cutting speed, 0.05 mm/rev feed rate and 0.2 mm depth of cut. In high-speed turning, increase in cutting speed reduces the cutting force. This happens due to the fact that increase in cutting speed induces a large amount of heat in plastic deformation zone resulting into softening of work material and thus requires smaller force to deform the chip [10]. On the other hand, maximum material removal rate was obtained at optimal process parameter settings, i.e., tool nose radius of 1.2 mm, cutting speed of 500 m/min, feed rate of 0.15 mm/rev and depth of cut of 0.6 mm. Generally, material removal rate depends on turning parameters. When higher cutting speed, depth of cut and feed rate were selected

Table 4 *S*/*N* ratio of different response variables

Exp. no	F_c	MRR	T_m	R_a
1	−35.22	12.02	−49.45	3.42
2	−44.34	23.98	−55.28	6.8
3	−49.18	30.98	−57.59	8.38
4	−34.06	13.00	−48.09	1.43
5	−42.64	25.02	−53.94	3.54
6	−48.40	32.01	−57.05	8.15
7	−39.87	19.90	−52.15	3.03
8	−45.81	29.40	−56.45	7.91
9	−36.81	23.47	−51.41	4.96
10	−44.00	21.44	−56.10	7.7
11	−38.63	18.01	−50.98	3.51
12	−45.85	27.51	−56.63	4.52
13	−40.08	18.98	−50.60	2.79
14	−46.72	28.49	−55.96	4.18
15	−41.67	22.55	−52.17	6.5
16	−42.06	23.38	−54.76	3.94
17	−38.92	19.95	−50.47	1.62
18	−45.05	29.45	−55.08	3.42

Table 3 Process parameters along with experimental results

Exp. no.	Process parameters				Response variables			
	R_n	V_c	V_f	d_p	F_c	MRR	T_m	R_a
1	0.8	400	0.05	0.2	57.68	3.99	297	0.457
2	0.8	400	0.1	0.4	164.90	15.83	581	0.674
3	0.8	400	0.15	0.6	287.83	35.43	758	0.952
4	0.8	450	0.05	0.2	50.47	4.47	254	0.381
5	0.8	450	0.1	0.4	135.60	17.82	498	0.565
6	0.8	450	0.15	0.6	263.16	39.87	712	0.830
7	0.8	500	0.05	0.4	98.53	9.89	405	0.412
8	0.8	500	0.1	0.6	195.37	29.53	665	0.725
9	0.8	500	0.15	0.2	69.34	14.91	372	0.635
10	1.2	400	0.05	0.6	158.63	11.81	638	0.705
11	1.2	400	0.1	0.2	85.45	7.96	354	0.473
12	1.2	400	0.15	0.4	196.30	23.74	679	0.618
13	1.2	450	0.05	0.4	101.03	8.90	339	0.402
14	1.2	450	0.1	0.6	216.87	26.58	628	0.594
15	1.2	450	0.15	0.2	121.30	13.42	406	0.667
16	1.2	500	0.05	0.6	126.80	14.76	547	0.591
17	1.2	500	0.1	0.2	82.36	9.94	334	0.391
18	1.2	500	0.15	0.4	178.87	29.68	568	0.635

Table 5 Mean of *S*/*N* ratio of different response variables

Level	R_n	V_c	V_f	d_c
S/*N* ratio of cutting force				
L1	−42.82	−42.87	−39.22	−37.56
L2	−42.56	−42.27	−42.85	−42.98
L3	–	−41.42	−44.50	−46.03
Optimal parameters: R_n2-V_c2-V_f1-d_c1				
S/*N* ratio of material removal rate				
L1	23.29	22.33	18.12	18.17
L2	23.34	23.35	24.15	24.14
L3	–	24.26	27.66	27.62
Optimal parameters: R_n2-V_c3-V_f3-d_c3				
S/*N* ratio of machining temperature				
L1	−53.64	−54.34	−51.86	−50.43
L2	−53.39	−52.97	−53.85	−53.95
L3	–	−53.39	−54.99	−56.32
Optimal parameters: R_n2-V_c2-V_f1-d_c1				
S/*N* ratio of surface roughness				
L1	5.18	5.72	3.55	3.41
L2	4.36	4.26	4.59	4.20
L3		4.34	6.17	6.71
Optimal parameters: R_n2-V_c2-V_f1-d_c1				

for turning, it increased contact length and developed high heat in machining zone, resulting in maximum work material removal in the form of chip [21].

3.2 Analysis of variance

Analysis of variance (ANOVA) is used to identify the significant effect of each process parameter on the response variables using MINITAB-14 statistical software. Table 6 represents the ANOVA result of individual response variable. In the ANOVA table, DoF denoted as degrees of freedom, Seq *SS* denoted as sum of squares, Adj MS denoted as mean squares, *P* denoted as probability, *C* % denoted as the percentage contribution of each process parameter. ANOVA was accomplished for 5% significance level (95% confidence level). When *P* value is less than 0.05 that means specific process parameter has significant effect on the particular response variable. According to ANOVA results, depth of cut is the major contributor to all response variables, which accounted for cutting force (62.3%), machining temperature (71.9%) and material removal rate (46.1%), respectively. Feed rate is second-dominant factor of all response variables during high-speed turning, which accounted for cutting force (28.5%), machining temperature (20.4%) and material removal rate (45.9%), respectively. Further, cutting speed is third-dominant factor of cutting force and machining temperature; its contribution in the response variables is 4.3% and 5.5%, respectively. Tool nose radius is not significantly affected on the above response variables, its contribution to the outcomes less than 1.8%. Further, Fig. 3 also shows the best combination of process parameters for each response variable by using main effect plot.

Cutting force is the most important technical aspect in machining as it helps to determine the machinability of work material and predict chip formation. In the present study, cutting force is considered as the major force component, which acts along the direction of cutting speed. According to ANOVA result, depth of cut and feed rate are most dominating factors of cutting force. As the depth of cut increases at lower cutting speed, the cutting force also increases. The reason is that maximum depth of cut causes the large contact area of cutting tool and work material interacts to each other, resulted in more friction between both surfaces of tool and workpiece caused large machining temperature developed in the cutting zone. Subsequently, more cutting force was required for material removal. Figure 3a, b shows the cutting force and machining temperature increases with increase in depth of cut and feed rate. Similarly, Lalwani et al. [22] also reported that depth of cut feed rate is significantly affected on the cutting force while finish turning of MCN250 steel and accounted in 52.60% and 41.64%, respectively. Recently, Santhanakrishnan et al. [23] pointed out machining temperature is significantly influence by depth of cut and feed rate. Figure 3a shows cutting force decreases with increase in cutting speed at lower feed rate and downfeed. The higher cutting speed induced huge temperature, which helps to soften work material near the plastic deformation zone. Hence, lower cutting force was obtained at higher cutting speed. Nalbant et al. [24] studied the effect of dry turning parameters on cutting force of Inconel 718 with ceramic tool. They found that cutting speed and depth of cut are significant factors affecting cutting force, and observed cutting speed increase 150–250 m/min causes 14.6% reduction in cutting force.

Material removal rate also greatly impacts on machining process because of its direct impact on productivity. MRR is known as the amount of material removed per unit time. In high-speed turning, MRR is calculated by Eq. 3.

$$\mathrm{MRR} = 1000 \times V_c \times V_f \times d_c. \tag{3}$$

Here, it is visible that, three major turning parameters such as cutting speed, feed rate and depth of cut are greatly influenced by the material removal rate. Further, Fig. 3c shows the *MRR* increase with increase in feed rate and depth of cut. This attributed to fact that increase in depth of cut is associated with high MRR during turning because cutting tool covers large machining area. Resulted in maximum material deformed into chip causes the shearing action on workpiece. On the other hand, feed rate is directly proportional to MRR since both factors depend on machining time.

Table 6 ANOVA of different response variables

Source	DoF	Seq SS	Adj MS	*F* value	*P*	*C* %
ANOVA of cutting force						
R_n	1	135	135	0.34	0.573	0.2
V_c	2	3252	1626	4.10	0.050	4.3
V_f	2	22,962	11,481	28.95	0.000	28.5
d_c	2	50,213	25,106	63.30	0.000	62.3
Error	10	3966	397			4.7
Total	17	80,529		R^2	95.07%	
ANOVA of material removal rate						
R_n	1	34.50	34.50	3.21	0.104	1.8
V_c	2	14.20	7.10	0.66	0.538	0.8
V_f	2	888.59	444.29	41.30	0.000	45.9
d_c	2	889.09	444.55	41.32	0.000	46.1
Error	10	107.58	10.76			5.4
Total	17	1933.96		R^2	94.43%	
ANOVA of machining temperature						
R_n	1	133	133	0.13	0.724	0.1
V_c	2	22,048	11,024	10.92	0.003	5.5
V_f	2	86,436	43,218	42.81	0.000	20.4
d_c	2	311,581	155,790	154.31	0.000	71.9
Error	10	10,096	1010			2.0
Total	17	430,295		R^2	97.65%	
ANOVA of surface roughness						
R_n	1	0.01742	0.01742	5.32	0.044	4.2
V_c	2	0.02321	0.01160	3.54	0.069	5.6
V_f	2	0.18111	0.09055	27.65	0.000	43.2
d_c	2	0.16407	0.08204	25.05	0.000	39.1
Error	10	0.03275	0.00327			7.9
Total	17	0.41857		R^2	92.07%	

Feed rate is defined as specific cutting tool movement over work material after one revolution. If feed rate increases, then faster cutting tool movement means minimum machining time required to remove the material. Hence, maximum MRR was obtained at higher feed rate. Similarly, Mai et al. [25] employed the *S*/*N* ratio and ANOVA to optimize the hard turning parameters for better machinability of AISI 1060 steel under MQL condition. They found that feed rate and depth of cut afflict the MRR mostly.

Table 6 shows the ANOVA result of surface roughness employed in high-speed turning. It is indicated that the feed rate (43.2%) exerts most dominant effect on surface roughness. The depth of cut (39.1%) exerts the second most significant factor, and lastly tool nose radius (4.2%) and cutting speed (5.6%). Figure 6d shows that surface roughness increases with increase in feed rate and depth of cut mostly. The reason is that the higher feed rate produced incomplete turning at faster traverse and generated chatter marks on finished surface. Resulted in higher surface roughness. In the same way, surface roughness drastically increases with increase in the depth of cut. This is happened due to large penetration of cutting tool in the hardened work material at higher depth of cut. Therefore, cutting tool undergoes extensive mechanical and thermal stress. This induces the flank wear and sometimes cutting tool broken. The same worn-out cutting tool is used for a long duration. This leads to higher surface roughness. Celik et al. [26] investigated the effect of different coated tungsten carbide tools on surface roughness and tool life while sustainable turning of Ti-6Al-4V. They observed that poor surface quality at higher feed rate and depth of cut owing to fracture PVD-coated tool rubbing over finished surface. As can be seen in Fig. 6d, the lower surface roughness was obtained at tool nose radius of 1.2 mm. It is well known that hypothetical surface roughness (R_a) is a function of tool nose radius and feed rate. This function can be rewritten as Eq. 4 [22].

$$R_a = \frac{V_f^2}{(32 \times R_n)}. \tag{4}$$

From Eq. 4, it is clearly that, a larger tool nose radius was created an excellent surface profile. If smaller tool nose

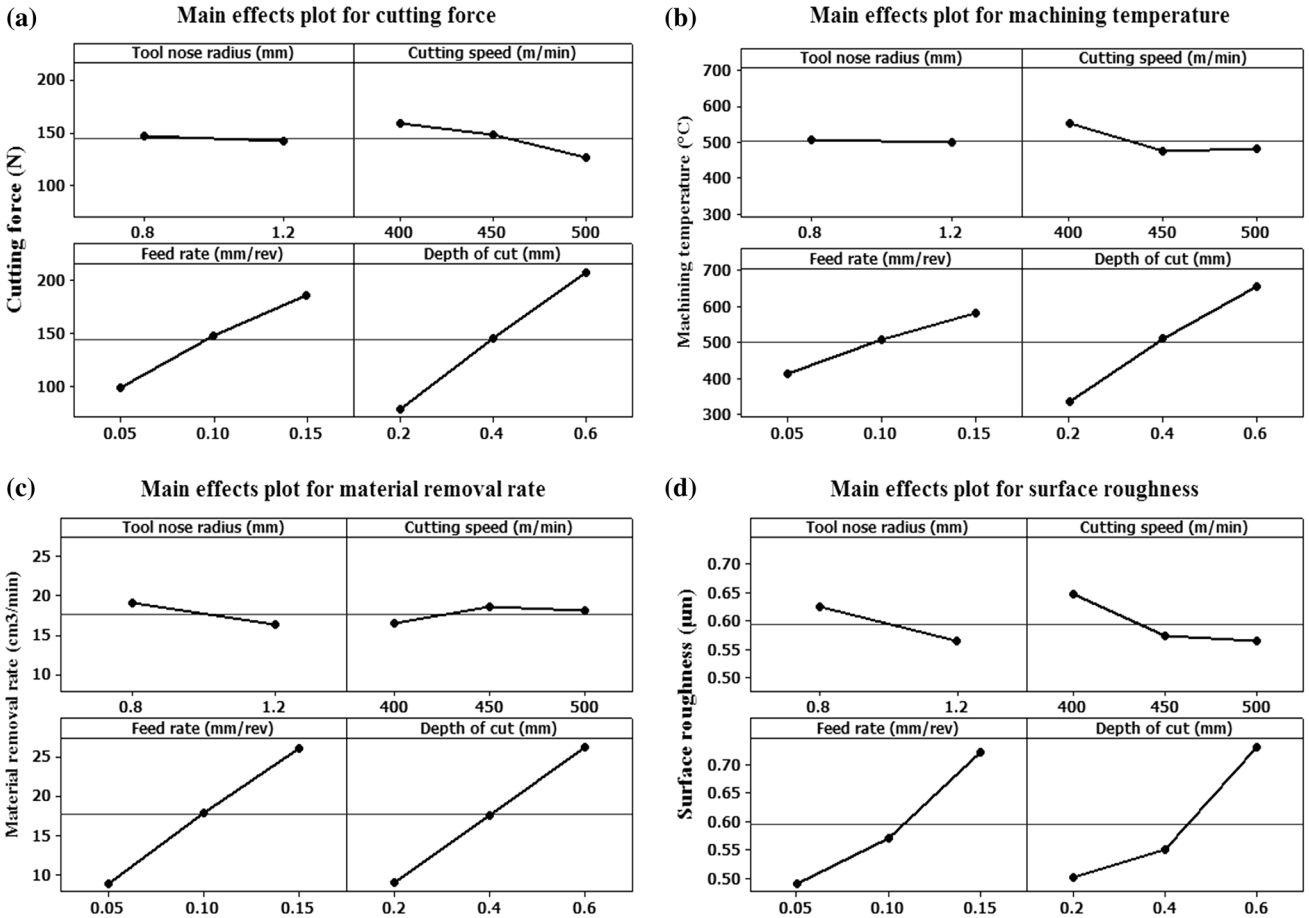

Fig. 3 Main effect plot of different response variables: **a** cutting force; **b** machining temperature; **c** material removal rate; **d** surface roughness

radius is utilized for high-speed turning of "difficult-to-cut" material, then cutting tool quickly wear-out owing to large heat effect on sharp cutting edge. Resulted in deep feed marks on the surface along with higher surface roughness was obtained at tool nose radius of 0.8 mm.

3.3 Grey relational analysis

S/*N* ratio method is adopted for optimization of turning parameters for single objective response variable. In many cases, objective of some response variables may be maximum or minimum value. In the present study, higher MRR is required to achieve maximum productivity, whereas lowest cutting force, machining temperature and surface roughness are required for better service life of the finished component. To address this issue, multi-objective optimization techniques are necessary to satisfy all response variables objective with optimal parameters conduction. Grey relational analysis (GRA) is the multi-objective response optimization technique, which developed by Deng in 1989 [27]. GRA commonly used for calculating the performance of variability of complex optimization problems with insufficient data. In the GRA, compare the original sequence and comparable sequence with the help of grey relational grade. The stepwise procedure of GRA is as follows:

3.3.1 Data pre-processing

Data pre-processing ($x_i^*(k)$) is the method of shifting experimental results from original sequence to comparable sequence. Whereas, the original data were normalized in the range of 0 and 1, to avoid the effect of response variable units and minimize the variability. This is called the grey relational generating [28]. Further, analysis was carried out on basis of normalization methods such as *S*/*N* ratio. In this study, material removal rate denoted as higher-to-better performance characteristics and is calculated using Eq. 5. Besides, cutting force, surface roughness and machining temperature were considered as lower-the-better performance characteristic and are determined by Eq. 6.

$$x_i^*(k) = \frac{x_i^*(k) - \min x_i^{(0)}(k)}{\max x_i^{(0)}(k) - \min x_i^{(0)}(k)} \tag{5}$$

$$x_i^*(k) = \frac{\max x_i^{(0)}(k) - x_i^{(0)}(k)}{\max x_i^{(0)}(k) - \min x_i^{(0)}(k)}, \tag{6}$$

whereas $x_i^{(0)}(k)$ is denoted as grey relational generation, $\max x_i^{(0)}(k)$ is maximum value of $x_i^*(k)$ for the kth responses, and $\min x_i^{(0)}(k)$ is minimum value of $x_i^*(k)$ for the kth responses. The normalized data of the different response variables are listed in Table 7. The highest value of normalized data represented as better performance characteristic and it is equal to one.

3.3.2 Determination of deviation sequences

The deviation sequence $\Delta 0_i(k)$ is the difference between the original sequence $x_i^*(k)$ and comparable sequence $x_i^*(k)$ after normalization. The deviation sequence of different response variables is given in Table 7. It is calculated by Eq. 7.

$$\Delta 0_i(k) = \left| x_0^*(k) - x_i^*(k) \right| \tag{7}$$

3.3.3 Estimation of grey relational coefficient

Grey relational coefficient (GRC) is applied to normalize data after deviation sequence for distributing experimental result in the best and worst condition according to important of response variables. When the two sequences settle at same points, then their GRC is 1. GRC can be expressed by Eq. 8 [29]:

$$\gamma(x_0(k), x_i(k)) = \frac{\Delta_{\min} + \xi \Delta_{\max}}{\Delta_{0i}(k) + \xi \Delta_{\max}} \tag{8}$$

whereas $\Delta_{\max}$ is maximum value of $\Delta 0_i(k)$=max. max $\Delta 0_i(k)$ and $\Delta_{\min}$ is minimum value of $\Delta 0_i(k)$=min. min $\Delta 0_i(k)$. ξ is denoted as distinguishing coefficient. Distinguishing coefficient value can be adjusted with the actual need and well defined in the range of 0 and 1 [30]. The calculated GRC is listed in Table 8.

3.3.4 Determination of weighted grey relational grade

The optimal value of multiple objective responses depends on grey relational grade (GRG). GRG is an average of grey relational coefficient corresponding to each response variable [28] and is calculated using Eq. 9:

$$\gamma\left(x_0, x_i\right) = \frac{1}{n} \sum_{i=1}^{n} \gamma\left(x_0(k), x_i(k)\right) \tag{9}$$

whereas $\gamma\left(x_0, x_i\right)$ denoted as grey relational grade of ith experiments and n denoted as number of response variables. GRG value indicates the level of relationship between the original sequence and comparable sequence. If the two sequences settle at same points, then their GRC is 1 and consequently, their GRG is equal to 1. According to importance of machined component in their industrial application, GRA was added weight of individual GRG. Weighted GRG can be determined according to Eq. 10 [31]:

Table 7 Data pre-processing and deviation sequences of different response variables

Exp. no	Data pre-processing				Deviation sequences			
	F_c	MRR	T_m	R_a	F_c	MRR	T_m	R_a
1	0.970	0.000	0.915	0.867	0.030	1.000	0.085	0.133
2	0.518	0.330	0.351	0.487	0.482	0.670	0.649	0.513
3	0.000	0.876	0.000	0.000	1.000	0.124	1.000	1.000
4	1.000	0.013	1.000	1.000	0.000	0.987	0.000	0.000
5	0.641	0.385	0.516	0.678	0.359	0.615	0.484	0.322
6	0.104	1.000	0.091	0.214	0.896	0.000	0.909	0.786
7	0.798	0.164	0.700	0.946	0.202	0.836	0.300	0.054
8	0.390	0.712	0.185	0.398	0.610	0.288	0.815	0.602
9	0.921	0.304	0.766	0.555	0.079	0.696	0.234	0.445
10	0.544	0.218	0.238	0.433	0.456	0.782	0.762	0.567
11	0.853	0.111	0.802	0.839	0.147	0.889	0.198	0.161
12	0.386	0.550	0.157	0.585	0.614	0.450	0.843	0.415
13	0.787	0.137	0.831	0.963	0.213	0.863	0.169	0.037
14	0.299	0.630	0.258	0.627	0.701	0.370	0.742	0.373
15	0.702	0.263	0.698	0.499	0.298	0.737	0.302	0.501
16	0.678	0.300	0.419	0.632	0.322	0.700	0.581	0.368
17	0.840	0.166	0.841	0.982	0.160	0.834	0.159	0.018
18	0.459	0.716	0.377	0.555	0.541	0.284	0.623	0.445

Table 8 Grey relational coefficient, weighted GRG and rank of each experiment

Exp. no.	Grey relational coefficient				Weighted GRG	Rank
	F_c	MRR	T_m	R_a		
1	0.943	0.333	0.854	0.790	0.169	5
2	0.509	0.427	0.435	0.494	0.117	17
3	0.333	0.802	0.333	0.333	0.118	16
4	1.000	0.336	1.000	1.000	0.200	1
5	0.582	0.449	0.508	0.608	0.137	9
6	0.358	1.000	0.355	0.389	0.141	7
7	0.712	0.374	0.625	0.902	0.174	4
8	0.450	0.634	0.380	0.454	0.125	14
9	0.863	0.418	0.681	0.529	0.136	10
10	0.523	0.390	0.396	0.468	0.111	18
11	0.772	0.360	0.716	0.756	0.159	6
12	0.449	0.527	0.372	0.546	0.128	13
13	0.701	0.367	0.748	0.931	0.180	3
14	0.416	0.574	0.403	0.573	0.135	11
15	0.626	0.404	0.624	0.500	0.124	15
16	0.609	0.417	0.462	0.576	0.130	12
17	0.758	0.375	0.759	0.966	0.187	2
18	0.480	0.638	0.445	0.529	0.137	8

$$\gamma_w(x_0, x_i) = \frac{1}{n}\sum_{i=1}^{n} w_1\left(\gamma\left(x_0(k), x_i(k)\right)\right) + w_2\left(\gamma\left(x_0(k), x_i(k)\right)\right) + w_3\left(\gamma\left(x_0(k), x_i(k)\right)\right) + w_4\left(\gamma\left(x_0(k), x_i(k)\right)\right) \tag{10}$$

whereas w_1, w_2, w_3, and w_4 are the weights of each response variable. According to die manufacturing industries, surface integrity is an important quality assurance factor because it decides acceptance or rejection of machined components on the basis of dimensional accuracy and surface quality as well as predict the service life of dies [32]. Hence, the maximum weightage was provided to surface roughness ($w_4 = 0.6$) followed by the material removal rate ($w_2 = 0.2$), cutting force and machining temperature (w_1, $w_3 = 0.1$), respectively. Second important response variable is material removal rate because it directly affects productivity, tooling cost and production cost. Cutting force and machining temperature depend on machining conditions and work material properties. Hence, equal weightage is given to them. Weighted GRG of each experiment is presented in Table 8.

3.3.5 Determination of optimal turning parameters

Higher weighted GRG indicated excellent performance characteristics of the combined response variables at optimal parameter setting. Table 8 clearly shows that experiment no. 4 is best experimental setting for high-speed turning of AISI S7 tool steel owing to higher weighted GRG (0.2). On the other hand, experiment no. 10 shows the worst turning conditions for hardened AISI S7 tool steel because of lowest weighted GRG. Further, the rank of the experiments was decided with the help of higher to lower value of weighted GRG. It is depicted in Table 8. Weighted GRG of each experiment sequence is considered as a single response variable for further study. The grey relational grade was optimized by Taguchi-based analysis of means. In analysis of mean, overall GRG grouping has been done initially by the parameter level for each column in the orthogonal array and then taking average of them on the basis of higher-to-better normalization criteria. Taguchi-based mean response of average-weighted GRG is listed in Table 9. From Table 9, optimal process parameters were selected for multi-objective response variables. Optimal parameter setting for overall response variable is $R_{n.}2$-$V_{c.}2$-$V_{f.}1$-$d_{p.}1$. In other word, optimal parameters such as tool nose radius of 1.2 mm, cutting

Table 9 Mean response table of weighted GRG

Level	R_n	V_c	V_f	d_c
Mean value of weighted GRG				
L1	0.143	0.134	0.161	0.162
L2	0.146	0.153	0.143	0.145
L3	–	0.148	0.131	0.126
Optimal parameters: $R_{n.}2$-$V_{c.}2$-$V_{f.}1$-$d_{c.}1$				

speed of 450 m/min, feed rate of 0.05 mm/rev and depth of cut of 0.2 mm for effective high-speed turning of AISI S7 tool steel. Figure 4 also shows the effect of turning parameters on weighted GRG of different response variables. The maximum weighted GRG was observed at higher tool nose radius, moderate cutting speed and lower feed rate and depth of cut. Similar results were observed by Pawade et al. [31], when implemented Taguchi-based weighted GRA to optimize the turning parameters for lower cutting force and surface roughness. They recommended higher cutting speed (475 m/min), lower feed rate (0.10 mm/rev) and lower depth of cut (0.5 mm) while high-speed turning of superalloy, Inconel 718. Furthermore, ANOVA was used to identify the level of significance of individual process parameter on multi-objective response variables. ANOVA result of GRG is summarized in Table 10. According to ANOVA result, it is seen that the depth of cut (33.04%), feed rate (23.80%), cutting speed (10.20%) and tool nose radius (0.33%) have significantly affected on the overall response characteristics. Depth of cut and feed rate were significantly affected on major weightage response variables like surface roughness and material removal rate. If feed rate and depth of cut increase, then tool-chip interface area increases, resulting in maximum material removal from work material. However, negative impact was observed on surface roughness. The higher feed rate and depth of cut were developed deeper feed marks and large side flow material over finished surface, resulting in higher surface roughness value [33].

3.3.6 Prediction of weighted GRG under optimal turning parameters

Confirmation test was performed on optimal process parameter setting to verify the best performance characteristics of hardened AISI S7 tool steel under high-speed turning. Optimal turning parameters are considered as input parameters for estimating the predicted weighted GRG value ($\gamma_{\text{predicted}}$). It is calculated by Eq. 11.

$$\gamma_{\text{predicted}} = \gamma_n + \sum_{i=1}^{N} (\gamma - \gamma_n) \tag{11}$$

whereas γ_n denoted as total mean of GRG, γ denoted as mean GRG of optimal process parameter, and N is denoted as the number of significant parameters that affect on response variables.

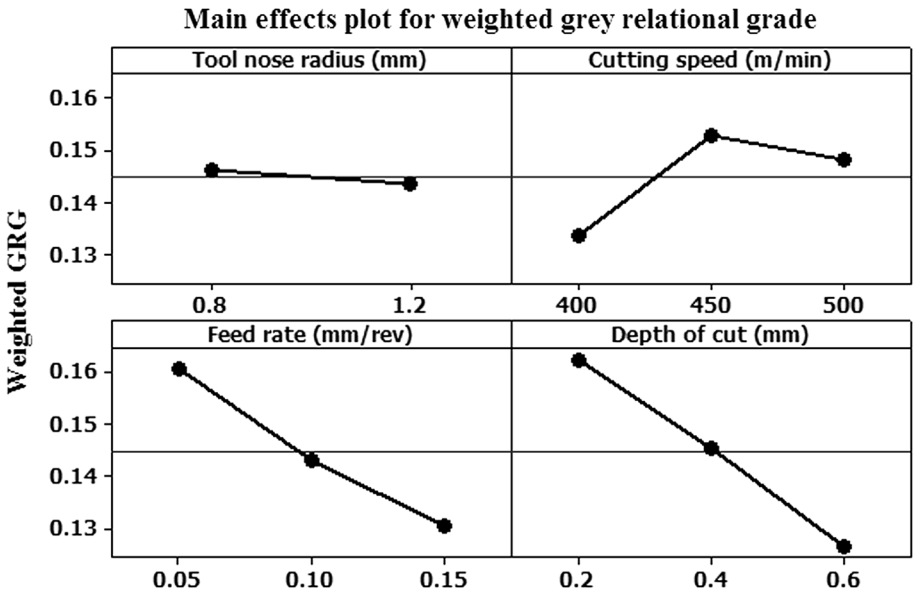

Fig. 4 Main effect plot of weighted grey relational grade

Table 10 ANOVA of weighted GRG

Source	DoF	Seq SS	Adj MS	*F* value	*P*	*C* %
R_n	1	0.00004	0.00004	0.09	0.770	0.33
V_c	2	0.00122	0.00060	1.48	0.271	10.20
V_f	2	0.00285	0.00136	3.42	0.068	23.80
d_c	2	0.00395	0.00193	4.71	0.035	33.04
Error	10	0.00391	0.00041			32.63
Total	17	0.01197				100

In the present study, optimal turning parameters, i.e., $R_{n.}2$-$V_{c.}2$-$V_{f.}1$-$d_{p.}1$ were estimated by weighted GRG mean analysis. ANOVA result of weighted GRG also clearly indicates depth of cut, feed rate and cutting speed are most influencing turning parameters. However, tool nose radius has less contribution to the multi-objective response variables. Hence, tool nose radius could not be considered for the prediction of weighted GRG. Only significant turning parameters ($N=3$) were accounted for the confirmation test. Predicted weighted GRG is 0.186. A confirmation test was performed three times on work material under optimal turning parameters setting. After this test, machining performance factors such as cutting force, material removal rate and machining temperature were 53.32 N, 4.47 cm^3/min and 275 °C, respectively. Surface roughness of work material is 0.409 µm. The experiment value of the weighted GRG at optimal turning parameter was 0.191. A confirmation test result was obtained by comparing initial turning parameter and optimal turning parameter and is listed in Table 11. It was found that the percentage improvement in weighted GRG is 21.38%. It is confirmed that GRA technique is effective optimization tool, which provides the optimal high-speed turning parameters for multi-objective response variables on hardened AISI S7 tool steel.

3.4 Tool wear

In high-speed turning, alumina-mixed ceramic insert was subjected to higher cutting speed, temperature and pressure around the nose radius, flank and rake side. This condition developed a thermo-mechanical effect on interaction surfaces of cutting tool, machined surface and nascent chip. Therefore, cutting tool has suffered an abrasion, adhesion and oxidation problems. Cutting tool wear evaluated in terms of flank and crater wear, notch wear, chip hammering, built-up edge formation and melted chips on the cutting tool. Figure 5 shows SEM micrographs of wear morphology of ceramic tool after turning of hardened AISI S7 tool steel under different process parameters. Generally, tool wear depends on machining parameters, hardness of work material and machining time [11]. As can be seen from Fig. 5a, the minimum flank wear was observed after machining time of 4 min at cutting speed of 400 m/min. In contrast, the maximum flank wear was observed after machining time of 4 min at cutting speed of 500 m/min, as shown in Fig. 5b. Further, notch and abrasion marks on the flank side were observed due to rubbing of hard and hot nascent chip over the flank surface at higher cutting speed. This sharp chip carries a small amount of material from flank side by abrasive action [34]. Figure 5c, d shows built-up edge (BUE) formation on the cutting edge of cutting tool at cutting speed of 400 m/min and feed rate of 0.15 mm/rev. When turning was performed at lower cutting speed and higher feed rate, which attributed to low heat development in cutting zone, resulted in insufficient deformation of work material. Therefore, few unstable chips welded at cutting edge and near the tool nose radius under thermo-mechanical loading condition [15]. The second reason for BUE formation on the ceramic tool is the unstable condition of TiC. Ceramic tool was made by the mixture of Al_2O_3 and TiC. Al_2O_3 is more stable at higher temperature. However, TiC remains unstable at higher temperature, which reacts with hardened AISI S7 tool steel. Resulted in work material sticks over the cutting tool. Aslantas et al. [35] also observed that BUE formed on Al_2O_3/TiCN-mixed ceramic tool while hard finish turning of hardened AISI 52100 steel. Figure 5c, d also shows the molten metal particle on the flank and rake surface. As can be seen in Fig. 5d, the crater wear was observed on the rake surface of cutting tool, but away from the cutting edge. This probably happens due to a change in rake angle as adhesion of work material initiates BUE formation on the cutting edge. This BUE changes the direction of chip flow away from the cutting edge on the rake surface. In addition, the chipping hammering effect was observed on the tool nose radius at depth of cut of 0.6 mm, feed rate of 0.15 mm/rev and cutting speed of 500 m/min, as shown in Fig. 5e, f. This wear phenomenon is complex character of diffusion wear. The large tool-work material interaction area caused by the higher feed rate and depth of cut during turning, which enhanced interaction of work material grain with cutting edge. Furthermore, large plastic deformed chip was applied thermo-mechanical loading on the tool nose radius under higher cutting speed. This resulted in drastic reduction in tool material strength owing to carbide element loss. Finally, tool nose radius was fractured after machining time of 4 min. The second reason of broken tool nose radius is occurrence of vibration during high-speed turning. When cutting speed of 500 m/min was applied for turning of work material for a long duration (more than 4 min), then cutting tool frequently hammered over hardened AISI S7 tool steel due to machine vibration. Resulted in fracture of tool nose radius. Similar results were observed by Pu et al. [36] while studying the

Table 11 Comparison between initial and optimal parameters

Response variables	Initial parameters	Optimal parameters	
		Prediction	Experimental
	$R_{n.}2$-$V_{c.}1$-$V_{f.}2$-$d_{c.}1$	$R_{n.}2$-$V_{c.}2$-$V_{f.}1$-$d_{c.}1$	$R_{n.}2$-$V_{c.}2$-$V_{f.}1$-$d_{c.}1$
F_c	85.45		53.32
MRR	7.97		4.47
T_m	354		275
R_a	0.473		0.409
Grade	0.159	0.186	0.193

Improvement in weighted GRG = 0.034

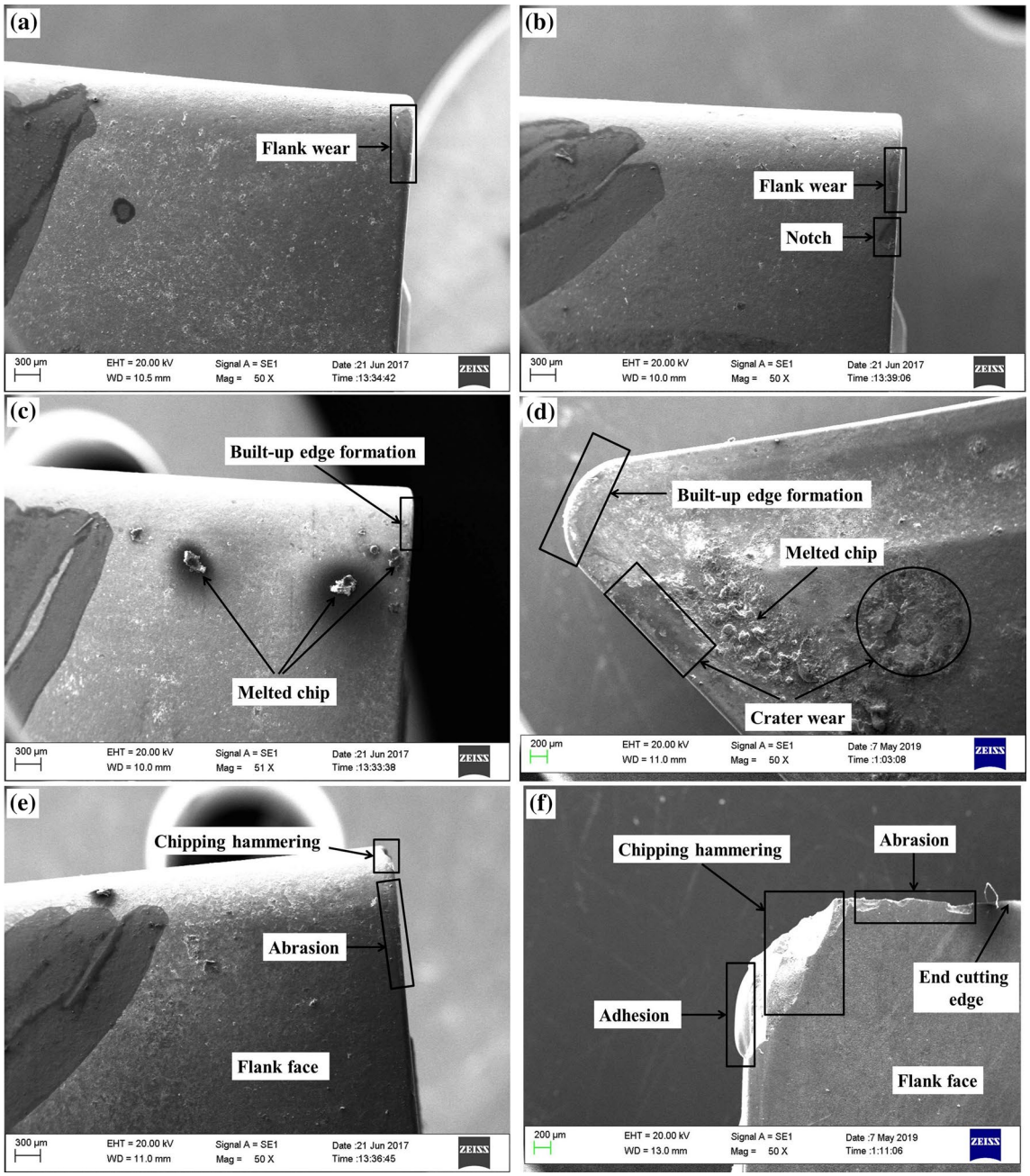

Fig. 5 SEM micrographs of exhibit failure of cutting tool under different turning conditions: **a** flank wear; **b** notch formation; **c** built-up edge formation; **d** crater wear; **e** chipping hammering effect; **f** broken tool

effect of higher cutting speed on the accelerating tool wear during turning of hardened AISI 1045 steel.

3.5 2D and 3D surface topography

Surface integrity plays an important role in working performance and service life of the machined component. It can be evaluated in terms of surface roughness and surface topography of machined surface. 2D surface topography was examined by SEM to study the effect of turning parameters and different tool wear modes on the finished surface. Figure 6 shows different machined surface defects including material side flow, redeposit metal, surface cavity, feed marks and smeared material. Figure 6a clearly shows the more surface damage in the form of large feed mark, material side flow and re-deposited metal at lower cutting speed and higher feed rate and depth of cut. This occurs due to maximum friction between the interaction surfaces of cutting tool, work material and nascent chip

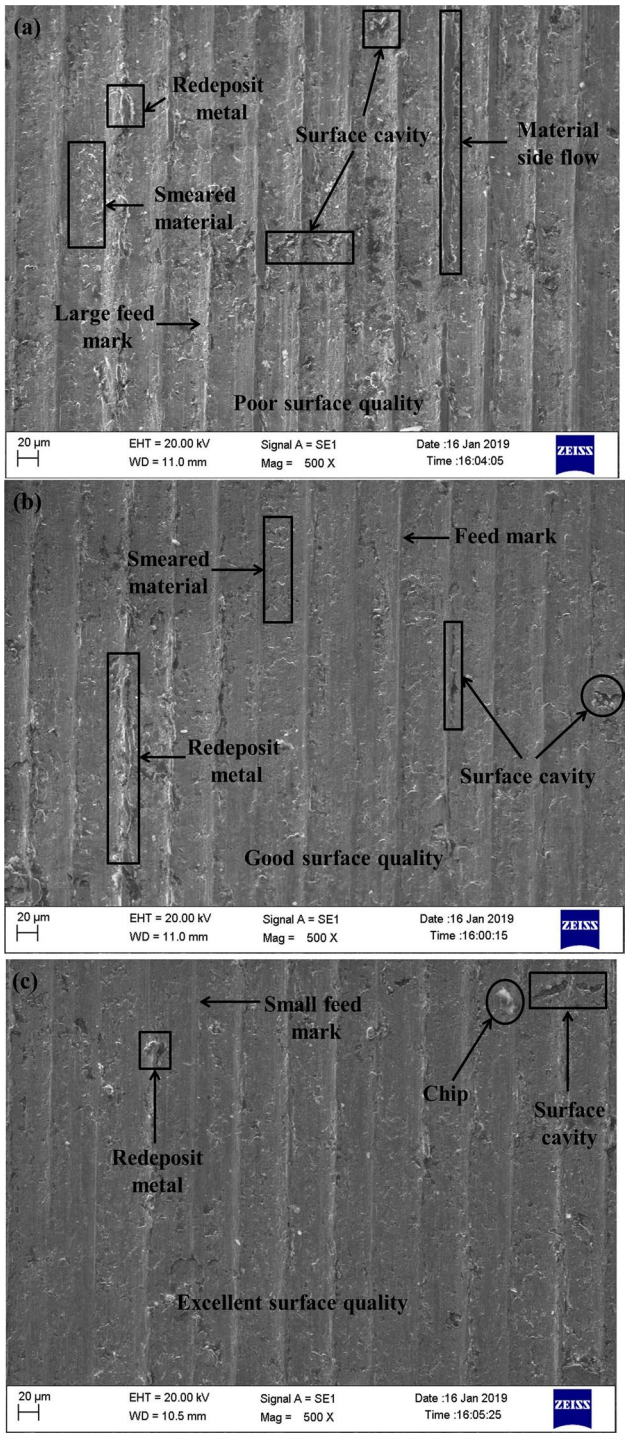

Fig. 6 SEM micrographs of machined sample under different cutting speed: **a** $V_c = 400$ m/min; **b** $V_c = 450$ m/min; **c** $V_c = 500$ m/min

at higher depth of cut and lower cutting speed, which induce high temperature in the machining zone. In addition, AISI S7 tool steel is sticky in nature. Resulted in redeposition of nascent chips over finished surface [10]. Further, large side flow material and deeper feed marks were noticed on the finished surface due to softening of work material at higher feed rate and cutting speed. Tool wear also significantly affected on the surface quality of the machined component. Material side flow defect was observed on finished surface owing to tool flank wear by thermo-mechanical loading. Recently, Liang and Liu [37] investigated the effect of tool flank wear on surface quality during high-speed machining of Ti-6Al-4V. They reported that poor surface finish along with high flank wear occurs due to large thermo-mechanical loads at tool/work interface. Figure 6a–c shows a common surface defect such as surface cavity was associated with all respective machined surface. Surface cavity was generated over finished surface due to carbide cracking [38]. In high-speed turning, large cutting speed and temperature are responsible for extensive oxidation of carbides from cutting tool and machined surface. This oxide layer could not sustain large strain produced between cutting tool and machined surface interface during turning. Hence, this carbide gets broken over the entire machined surface. These broken carbides leave some cavity on the finished surface. The smeared surface defect was observed in all respective machined surface at higher cutting speed because the broken carbide particles were re-deposited on finished surface and pull-out some carbides from finished surface by cutting tool during second pass of turning [39]. Figure 6c indicates that excellent surface finish was observed at higher cutting speed as well as lower feed rate and depth of cut. However, small debris embedded on finished surface due to microstructural inhomogeneity of debris at higher temperature.

2D surface topography and surface roughness parameters provided limited information about the machined surface, whereas 3D surface topography described the integral features of machined surface like depth of groove and material side flow area with nanoscale surface roughness. For measurement of 3D surface roughness profile, cantilever probe moved over machined surface up to 50 µm along to feed direction. 3D surface roughness was evaluated in the teams of average arithmetical height (S_a), root mean square deviation (S_q) and maximum peak-to-valley height (S_t). It can be calculated using Eqs. 12, 13 [37].

$$S_a = \frac{1}{P}\iint_P^1 |z(x,y)|\mathrm{d}x\mathrm{d}y \tag{12}$$

$$S_q = \sqrt{\frac{1}{P}\iint_P^1 z^2(x,y)\mathrm{d}x\mathrm{d}y} \tag{13}$$

whereas P is denoted as the analyzed area, x, y *is* denoted as mean of analyzed area, sis denoted as the average of finished surface height.

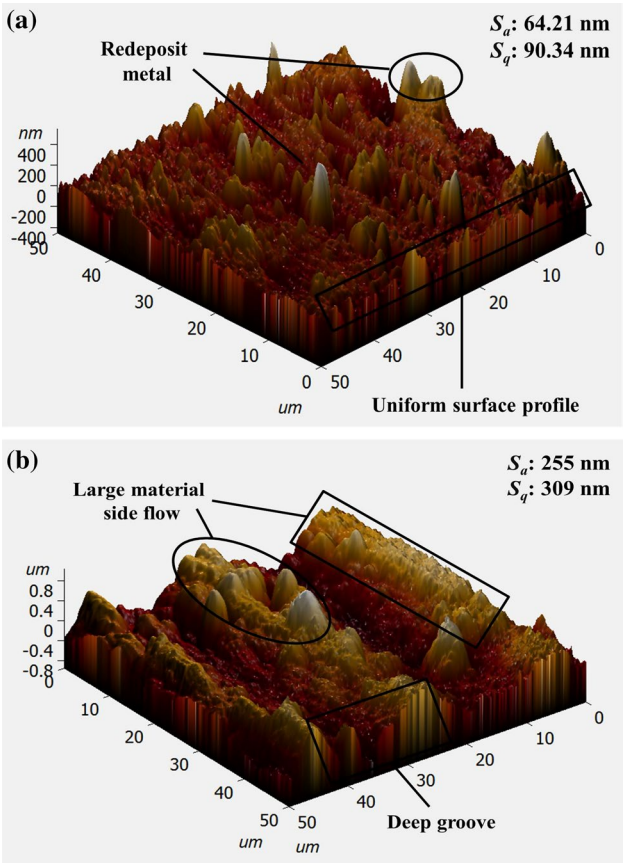

Fig. 7 3D surface topography under different turning condition: **a** best; **b** worst

Figure 7 shows the 3D micro-topography of finished surface under best and worst turning condition. Figure 7a depicts that uniform surface profile with negligible re-deposited metal was obtained upon turning of AISI S7 tool steel at cutting speed of 450 m/min, feed rate of 0.05 mm/rev, depth of cut of 0.2 mm and tool nose radius of 0.8 mm (refer experiment no. 4). This is attributed to the higher level of plasticity in work material owing to localized heating in the cutting zone at higher cutting speed. This helps to carry away the soft chip from finished surface. In addition, minimum surface roughness (S_a: 64.21 nm, S_q: 90.34 nm, and S_t: 1008 nm) was obtained under best turning condition. On the other hand, poor machined surface quality was observed at feed rate of 0.15 mm/rev, depth of cut of 0.6 mm, cutting speed of 400 m/min and tool nose radius of 0.8 mm (refer experiment no. 3). Figure 7b shows the deeper grooves and large material side flow on the finished surface because of feed rate and depth of cut are the most dominant factors of surface quality followed by cutting speed and tool nose radius. Maximum surface roughness (S_a: 309 nm, S_q: 255 nm and S_t: 1977 nm) was obtained under worst turning condition. Similarly, Babu et al. [40] also adopted 3D surface topography method for machined surface characterization after copper nanofluid-based finishing turning of EN 24 steel.

4 Conclusions

The main conclusions can be made from the present research work:

1. According to *S*/*N* ratio, optimal turning parameters for higher material removal rate were tool nose radius of 1.2 mm, cutting speed of 500 m/min, feed rate of 0.15 mm/rev and depth of cut 0.6 mm. In contrast, the lowest cutting force, machining temperature and surface roughness were obtained at optimal turning parameters including tool nose radius of 1.2 mm, cutting speed of 450 m/min, feed rate of 0.05 mm/rev and depth of cut of 0.2 mm.
2. ANOVA result indicated that, depth of cut and feed rate are most significant turning parameters for each response variable followed by cutting speed and tool nose radius. Besides, lower surface roughness was obtained at higher cutting speed and tool nose radius.
3. According to GRA analysis, higher weighted grey relational grade (0.20) was obtained at optimal process parameters setting, i.e., $R_n = 1.2$ mm, $V_c = 450$ m/min, $V_f = 0.05$ mm/rev, and $d_c = 0.2$ mm. These parameters were recommended to high-speed turning of hardened AISI S7 tool steel for better multi-performance response variables.
4. SEM and AFM micrograph clearly shows excellent surface quality with lowest surface roughness (S_a: 64.21 nm, S_q: 90.34 nm) was obtained at higher cutting speed and lower feed rate.
5. Flank wear and notch depth gradually increase with increase in cutting speed owing to thermo-mechanical loading. However, crater wear occurred on the rake face at lower cutting speed. Lastly, tool nose radius was fractured at higher depth of cut and cutting speed owing to diffusion wear.

Acknowledgements The authors would like to thank Government of India and technical education quality improvement programmer (TEQIP) for providing financial support and experimental facility at Advanced Manufacturing Lab, Walchand College of Engineering, Sangli. Authors are also thankful to Dr. Meghanshu Vashista and Dr. Modh Zaheer khan Yusufzai for providing surface characterization facility at Central Instrument Facility Centre, Indian Institute of Technology (BHU), Varanasi.

References

1. Pfefferkorn FE, Duffie NA, Morrow JD, Wang Q (2014) Effect of beam diameter on pulsed laser polishing of S7 tool steel. CIRP Ann 63(1):237–240
2. Morrow JD, Pfefferkorn FE (2016) Local microstructure and hardness variation after pulsed laser micromelting on S7 tool steel. J Micro Nano-Manuf 4(3):031006
3. Soković M, Mijanović K (2001) Ecological aspects of the cutting fluids and its influence on quantifiable parameters of the cutting processes. J Mater Process Technol 109(1–2):181–189
4. Awale A, Inamdar K (2015) Review on high speed machining of hard material. J Emerg Technol Innov Res 2(3):517–524
5. Dudzinski D, Devillez A, Moufki A, Larrouquere D, Zerrouki V, Vigneau J (2004) A review of developments towards dry and high speed machining of Inconel 718 alloy. Int J Mach Tool Manuf 44(4):439–456
6. Iuliano L, Settineri L, Gatto A (1998) High-speed turning experiments on metal matrix composites. Compos A Appl Sci Manuf 29(12):1501–1509
7. Kishawy H, Elbestawi M (2001) Tool wear and surface integrity during high-speed turning of hardened steel with polycrystalline cubic boron nitride tools. Proc Inst Mech Eng Part B J Eng Manuf 215(6):755–767
8. Abukhshim N, Mativenga P, Sheikh M (2005) Investigation of heat partition in high speed turning of high strength alloy steel. Int J Mach Tool Manuf 45(15):1687–1695
9. Pawade R, Joshi SS, Brahmankar P, Rahman M (2007) An investigation of cutting forces and surface damage in high-speed turning of Inconel 718. J Mater Process Technol 192:139–146
10. Thakur D, Ramamoorthy B, Vijayaraghavan L (2009) Study on the machinability characteristics of superalloy Inconel 718 during high speed turning. Mater Design 30(5):1718–1725
11. Zhou J, Bushlya V, Stahl J (2012) An investigation of surface damage in the high speed turning of Inconel 718 with use of whisker reinforced ceramic tools. J Mater Process Technol 212(2):372–384
12. Naskar A, Chattopadhyay A (2018) Investigation on flank wear mechanism of CVD and PVD hard coatings in high speed dry turning of low and high carbon steel. Wear 396:98–106
13. Tzeng C-J, Lin Y-H, Yang Y-K, Jeng M-C (2009) Optimization of turning operations with multiple performance characteristics using the Taguchi method and Grey relational analysis. J Mater Process Technol 209(6):2753–2759
14. Kacal A, Yıldırım F (2013) Application of grey relational analysis in high-speed machining of hardened AISI D6 steel. Proc Inst Mech Eng Part C J Mech Eng Sci 227(7):1566–1576
15. Eskandari B, Davoodi B, Ghorbani H (2018) Multi-objective optimization of parameters in turning of N-155 iron-nickel-base superalloy using gray relational analysis. J Braz Soc Mech Sci 40(4):233
16. Ghetiya N, Patel K, Kavar A (2016) Multi-objective optimization of FSW process parameters of aluminium alloy using Taguchi-based grey relational analysis. Trans Indian Inst Met 69(4):917–923
17. Pandey AK, Gautam GD (2018) Grey relational analysis-based genetic algorithm optimization of electrical discharge drilling of Nimonic-90 superalloy. J Braz Soc Mech Sci 40(3):117
18. Bhatt RJ, Raval HK (2018) Investigation on flow forming process using Taguchi-based grey relational analysis (GRA) through experiments and finite element analysis (FEA). J Braz Soc Mech Sci 40(11):531
19. Mp GC, Krishna P, Parappagoudar MB (2014) Optimization of squeeze cast process parameters using Taguchi and grey relational analysis. Procedia Technol 14:157–164
20. Ross PJ, Ross PJ (1988) Taguchi techniques for quality engineering: loss function, orthogonal experiments, parameter and tolerance design. vol TS156 R12. McGraw-Hill, New York
21. Thakur D, Ramamoorthy B, Vijayaraghavan L (2009) A study on the parameters in high-speed turning of superalloy Inconel 718. Mater Manuf Process 24(4):497–503
22. Lalwani DI, Mehta NK, Jain PK (2008) Experimental investigations of cutting parameters influence on cutting forces and surface roughness in finish hard turning of MDN250 steel. J Mater Process Technol 206(1):167–179
23. Santhanakrishnan M, Sivasakthivel P, Sudhakaran R (2017) Modeling of geometrical and machining parameters on temperature rise while machining Al 6351 using response surface methodology and genetic algorithm. J Braz Soc Mech Sci 39(2):487–496
24. Nalbant M, Altın A, Gökkaya H (2007) The effect of cutting speed and cutting tool geometry on machinability properties of nickel-base Inconel 718 super alloys. Mater Design 28(4):1334–1338
25. Mia M, Dey PR, Hossain MS, Arafat MT, Asaduzzaman M, Ullah MS, Zobaer ST (2018) Taguchi *S/N* based optimization of machining parameters for surface roughness, tool wear and material removal rate in hard turning under MQL cutting condition. Measurement 122:380–391
26. Celik YH, Kilickap E, Güney M (2017) Investigation of cutting parameters affecting on tool wear and surface roughness in dry turning of Ti-6Al-4V using CVD and PVD coated tools. J Braz Soc Mech Sci 39(6):2085–2093
27. Deng J (1989) Introduction to grey system theory. J Grey Syst 1(1):1–24
28. Lin J, Lin C (2002) The use of the orthogonal array with grey relational analysis to optimize the electrical discharge machining process with multiple performance characteristics. Int J Mach Tool Manuf 42(2):237–244
29. Ng DK (1994) Grey system and grey relational model. ACM SIGICE Bull 20(2):2–9
30. Ren J, Zhai Z, Shi K, Zhou J, Yang J, Cai J (2018) Tool determination and geometry parameter optimization of carbide tool in high-speed milling of third-generation γ-TiAl alloy. J Braz Soc Mech Sci 40(10):491
31. Pawade RS, Joshi SS (2011) Multi-objective optimization of surface roughness and cutting forces in high-speed turning of Inconel 718 using Taguchi grey relational analysis (TGRA). Int J Adv Manuf Technol 56(1–4):47–62
32. Reinhall P, Ghassaei S, Choo V (1988) An analysis of rivet die design in electromagnetic riveting. J Vib Acoust Stress Reliab Des 110(1):65–69
33. Kishawy H, Elbestawi M (1999) Effects of process parameters on material side flow during hard turning. Int J Mach Tool Manuf 39(7):1017–1030
34. Zheng G, Xu R, Cheng X, Zhao G, Li L, Zhao J (2018) Effect of cutting parameters on wear behavior of coated tool and surface roughness in high-speed turning of 300M. Measurement 125:99–108
35. Aslantas K, Ucun İ, Çicek A (2012) Tool life and wear mechanism of coated and uncoated Al_2O_3/TiCN mixed ceramic tools in turning hardened alloy steel. Wear 274–275:442–451
36. Pu CL, Zhu G, Yang SB, Yue EB, Subramanian SV (2016) Effect of dynamic recrystallization at tool-chip interface on accelerating tool wear during high-speed cutting of AISI 1045 steel. Int J Mach Tool Manuf 100:72–80

37. Liang X, Liu Z (2018) Tool wear behaviors and corresponding machined surface topography during high-speed machining of Ti-6Al-4V with fine grain tools. Tribol Int 121:321–332
38. Zhou J, Bushlya V, Avdovic P, Ståhl JE (2012) Study of surface quality in high speed turning of Inconel 718 with uncoated and coated CBN tools. Int J Adv Manuf Technol 58(1):141–151
39. Chen Z, Lin Peng R, Zhou J, M'Saoubi R, Gustafsson D, Moverare J (2019) Effect of machining parameters on cutting force and surface integrity when high-speed turning AD 730™ with PCBN tools. Int J Adv Manuf Technol 100(9):2601–2615
40. Babu MN, Anandan V, Muthukrishnan N (2019) Analysis of EN24 steel in turning process with copper nanofluids under minimum quantity lubrication. J Braz Soc Mech Sci 41(2):101